Science of the Total Environment 656 (2019) 70–79

Contents lists available at ScienceDirect

Science of the Total Environment

journal homepage: www.elsevier.com/locate/scitotenv

Mechanisms of graphene oxide aggregation, retention, and release in quartz sand

Yan Liang [a], Scott A. Bradford [b,*], Jiří Šimůnek [c], Erwin Klumpp [d]

[a] School of Resources, Environment and Materials, Guangxi University, Nanning, China
[b] US Salinity Laboratory, USDA, ARS, Riverside, CA, United States
[c] Department of Environmental Sciences, University of California, Riverside, CA, United States
[d] Agrosphere Institute, IBG-3, Forschungszentrum Jülich GmbH, Jülich, Germany

HIGHLIGHTS

- GO interaction depended on GO geometry and orientation, roughness, and adsorbed Ca^{2+}.
- GO interacted in a shallow primary minimum under low ionic strength conditions.
- Level arms from roughness and grain-grain contacts were important for GO retention.
- A mathematical model interpreted the aggregation, retention, and release of GO.

GRAPHICAL ABSTRACT

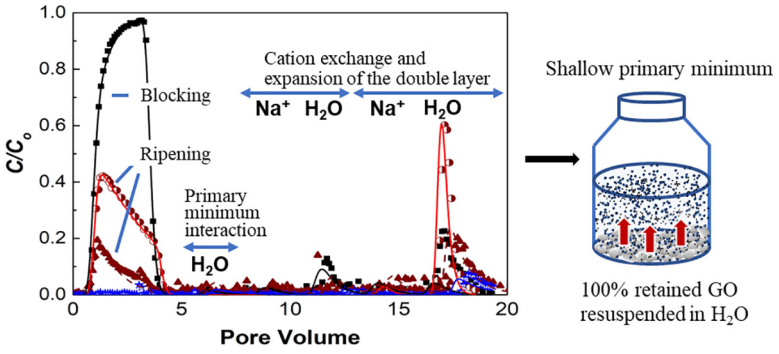

ARTICLE INFO

Article history:
Received 12 October 2018
Received in revised form 15 November 2018
Accepted 17 November 2018
Available online 22 November 2018

Editor: Kevin V. Thomas

Keywords:
Graphene oxide
Aggregation
Release
Blocking
Ripening

ABSTRACT

The roles of graphene oxide (GO) particle geometry, GO surface orientation, surface roughness, and nanoscale chemical heterogeneity on interaction energies, aggregation, retention, and release of GO in porous media were not fully considered in previous studies. Consequently, mechanisms controlling the environmental fate of GO were incompletely or inaccurately quantified. To overcome this limitation, plate-plate interaction energies were modified to account for these factors and used in conjunction with a mathematical model to interpret the results of GO aggregation, retention, and release studies. Calculations revealed that these factors had a large influence on the predicted interaction energy parameters. Similar to previous literature, the secondary minimum was predicted to dominate on smooth, chemically homogeneous surfaces that were oriented parallel to each other, especially at higher ionic strength (IS). Conversely, shallow primary minimum interactions were sometimes predicted to occur on surfaces with nanoscale roughness and chemical heterogeneity due to adsorbed Ca^{2+} ions, especially when the GO particles were oriented perpendicular to the interacting surface. Experimental results were generally consistent with these predictions and indicated that the primary minimum played a major role in GO retention and the secondary minimum contributed to GO release with IS reduction. Cation exchange (Na^{+} replacing Ca^{2+}) enhanced GO release with IS reduction when particles were initially deposited in the presence of Ca^{2+} ions. However, retained GO were always completely recovered into the excess deionized water when the sand pore structure was destroyed during excavation, and this indicates that primary minima were shallow and that the pore structure also played an important role in GO retention. Further evidence for the

* Corresponding author.
E-mail address: scott.bradford@ars.usda.gov (S.A. Bradford).

https://doi.org/10.1016/j.scitotenv.2018.11.258

role of pore structure on GO retention was obtained by conducting experiments in finer textured sand and at higher input concentrations that induced greater aggregation. In both cases, greater GO retention occurred, and retention profiles became more hyperexponential in shape.

1. Introduction

Graphene oxide (GO) is an oxidized form of graphene-based nanomaterial that contains reactive oxygen functional groups, such as hydroxyl, carbonyl, carboxyl and phenol (Dreyer et al., 2010). GO has found widespread use in industrial applications because of its excellent electrochemical properties (Zhu et al., 2010). A number of studies have also investigated the use of GO for pollutant removal in groundwater, surface water, and wastewater (Wang et al., 2013; He et al., 2018). However, there is concern about the inevitable release of GO into the environment due to its potential to adversely influence organisms, cells, and ecosystems (Guo and Mei, 2014; Liu et al., 2011).

A number of physicochemical factors are known to influence the aggregation, transport, retention, and release of GO in porous media (He et al., 2017). Commonly examined effects of solution chemistry on GO environmental fate include the ionic strength (IS) (Dong et al., 2016; Dong et al., 2017; Fan et al., 2015a; Lanphere et al., 2013; Lanphere et al., 2014; Liu et al., 2013; Qi et al., 2014; Wang et al., 2017a; Wang et al., 2018; Wu et al., 2013b; Xia et al., 2015) and cation type (Fan et al., 2015b; Wang et al., 2017a; Wang et al., 2018; Xia et al., 2015). An increase in solution IS has been reported to increase GO aggregation and retention in porous media due to the compression of the double layer thickness and charge screening which increases the depth of the secondary minimum (Dong et al., 2016; Lanphere et al., 2013; Liu et al., 2013; Wang et al., 2017a; Wang et al., 2018; Xia et al., 2015). Divalent cations have been reported to increase GO aggregation and retention due to cation bridging (Fan et al., 2015b; Wang et al., 2018; Wu et al., 2013a; Xia et al., 2015).

Previous GO transport studies that have conducted interaction energy calculations assumed smooth and chemically homogeneous surfaces to interpret their results (Chowdhury et al., 2014; Dong et al., 2016; Feriancikova and Xu, 2012; Liu et al., 2013; Wang et al., 2017a; Wang et al., 2018; Wu et al., 2013b; Xia et al., 2015). In this case, GO interactions were mainly attributed to secondary minimum interactions (Dong et al., 2016; Liu et al., 2013; Wang et al., 2017a; Wang et al., 2018; Xia et al., 2015). A decrease in the solution IS to deionized (DI) water should eliminate the secondary minimum and induce disaggregation or release of retained particles (Shen et al., 2018; Torkzaban and Bradford, 2016; Wang et al., 2017a). Indeed, release pulses of previously retained GO have been observed in column studies when the IS was reduced to DI water (Dong et al., 2016; Lanphere et al., 2014; Wang et al., 2017a). However, only a fraction of the retained GO particles was released when the IS was reduced to DI water, especially when GO particles were deposited in the presence of divalent cations (Dong et al., 2016; Wang et al., 2017a). Interaction energy calculations on smooth, chemically homogeneous surfaces also cannot explain the enhanced GO aggregation and retention in the presence of divalent cations at low IS (Fan et al., 2015b; Wang et al., 2018; Wu et al., 2013a; Xia et al., 2015), or complete recovery of retained GO following sand excavation (Lanphere et al., 2014; Sun et al., 2015; Wang et al., 2017a). These observations indicate that other factors were contributing to the GO retention and release besides the secondary minimum.

One potential explanation for these deviations between conventional interaction energy predictions and experimental observations is due to violation of assumptions in these calculations. In particular, nanoscale surface roughness and chemical heterogeneity have been shown to have a large influence on interaction energy parameters (Bendersky and Davis, 2011; Bhattacharjee et al., 1998; Bradford et al., 2017; Bradford and Torkzaban, 2012). For example, the presence of nanoscale roughness and/or chemical heterogeneity can locally reduce and/or eliminate the energy barrier on electrostatically unfavorable surfaces (Bendersky and Davis, 2011; Bhattacharjee et al., 1998; Bradford and Torkzaban, 2013; Henry et al., 2011; Hoek and Agarwal, 2006; Suresh and Walz, 1996), and nanoscale roughness can dramatically reduce the depths of the secondary and primary minima, especially when roughness occurs on both surfaces (Bradford et al., 2017; Bradford et al., 2018). Shen et al. (2018) demonstrated that spherical colloids could attach in a primary minimum on concave and/or convex surfaces under unfavorable electrostatic conditions, with convex locations being more hydrodynamically favorable. Furthermore, GO requires additional modification to conventional interaction energy calculations to account for its finite plate geometry and orientation with the surface. Wu et al. (2013a) demonstrated that the interaction energy for multi-walled carbon nanotubes was sensitive to its orientation with the interacting surface. Wang et al. (2017a) showed how the plate structure of GO could be accounted for in interaction energy calculations but did not consider the influence of this structure during aggregation or the orientation of the plate with the surface. No studies have considered the role of surface roughness and chemical heterogeneity in conjunction with GO plate geometry and surface orientation. This information is needed to accurately predict the adhesive interactions that contribute to GO aggregation, retention, and release.

The GO input concentration (C_o) can also potentially influence GO aggregation and retention through several different processes that are not fully understood or quantified. For example, an increase in the suspension concentration is expected to increase the frequency of collisions and aggregation (Lee, 1983), although this effect has not yet been examined for GO suspensions. Conversely, an increase in C_o has also been reported to decrease the retention rate coefficient and enhance GO transport because of more rapid filling/blocking of available retention sites (Sun et al., 2015). Blocking has commonly been observed in GO transport studies (Lanphere et al., 2014; Sun et al., 2015; Wang et al., 2017a). Aggregating GO suspensions have been associated with increased straining, ripening behavior (a decrease in effluent concentration with continued GO injection), and changes in the particle size distribution during transport. For example, straining is expected to increase with increasing aggregate size, decreasing grain size, and to produce retention profiles with a more hyperexponential shape (Bradford et al., 2003). Ripening of GO has sometimes been observed to occur under higher IS conditions and in the presence of divalent cations (Lanphere et al., 2014). The average particle size of GO has been found to increase during transport through porous media, although a smaller GO particle size and more retention was observed in finer textured sand due to an increase in the GO mass transfer to the solid phase (Sun et al., 2015). However, decreasing GO retention with a decreasing sand size has also been reported and attributed to an increase in hydrodynamic shear force (Wang et al., 2017b). These conflicting findings indicate that further research is needed to clarify the roles of C_o and grain size on GO retention.

The objective of this study is to clarify the mechanisms of aggregation, retention, and release of GO in porous media under various physicochemical conditions, including IS, cation type, C_o, and grain size. This data was interpreted using novel interaction energy calculations and an advanced model that considered advection and dispersion transport, first-order retention, blocking or ripening, and transient (IS reduction and cation exchange) release. The interaction energy calculations for GO-GO and GO-sand accounted for the plate geometry of GO, horizontal and vertical orientations of the GO plate with a surface, and nanoscale

roughness and chemical heterogeneity on both the solid water interface and GO. These interaction energy calculations, retention and transient release experiments, and retention profiles were used to better infer the mechanisms of GO retention and release. Additional aggregation and transport studies were conducted at different C_o and grain sizes to improve our understanding of the influence of concurrent aggregation on time- (blocking or ripening) and depth-dependent (hyperexponential retention profiles) retention, and straining processes. The collected data provides valuable insight into the mechanisms of aggregation, retention, and release of GO and other particles (e.g., clays) with plate structure. This information is important for the assessment of the fate of GO in soil and groundwater environments.

2. Materials and methods

2.1. Solution chemistry and porous media

Electrolyte solutions were made using DI water and NaCl or $CaCl_2$ (analytical reagent) with various solution IS, i.e., different concentrations of 1, 10, 20, 50, 75, 100, 150, and 200 mM NaCl or 0.10, 0.20, 0.33, 0.40, 0.50, 0.60, 0.70, 0.83, 1.67, 2.50, and 3.33 mM $CaCl_2$. These solutions were unbuffered and the pH ranged from around 7 to 8.

Three sizes of analytically pure quartz sand (Sinopharm Chemical Reagent CO., Ltd., China) were employed in column experiments, with median grain sizes of 1090, 519, or 330 μm. To minimize the trace amount of metal oxides and organic impurities that can occur in quartz sand, purification procedures were conducted before sand column packing (Fan et al., 2015a). The surface charge characteristics of the purified sand were determined using a ZetaSizer Nano ZS90 (Malvern Instruments, Worcestershire, U.K.) after it had been milled into powders and placed in selected NaCl or $CaCl_2$ solutions.

2.2. GO suspensions

The raw GO suspension (2 g L^{-1}) was purchased from Carmery Materials Technology Co. Ltd., Shanxi, China. Information on the surface characterization of these GO particles (e.g., AFM, FT-IR, Raman spectra, and XPS) is already provided in the literature (Xia et al., 2017). The suspension for each experiment was freshly prepared by diluting the raw concentrated GO suspension into a selected NaCl or $CaCl_2$ solution to achieve an approximate concentration of 5, 10, 50, or 100 mg L^{-1} GO. The GO suspension was shaken by hand and then sonicated for 15 min in a sonication bath. The ZetaSizer apparatus was used to measure the hydrodynamic diameter and the zeta potential of GO suspensions.

Aggregation experiments were conducted by measuring the hydrodynamic diameter of GO in the suspension every 5 s over a 50 min duration with the ZetaSizer. The aggregation rate and attachment efficiency were calculated using Eqs. (S1)–(S3).

Concentrations of GO were determined using a UV–Vis spectrophotometer (Thermo ScientificTM Evolution 300, U.S.) at a wavelength of 230 nm. GO concentrations were evaluated using a calibration curve between the absorbance and standard solutions ($R^2 > 0.9995$).

2.3. Column experiments

2.3.1. Transport experiments

Saturated transport experiments were performed following similar procedures to our previous study (Liang et al., 2013). In brief, a stainless-steel column with a 3 cm inner diameter and a 12 cm length was wet-packed with quartz sand. The background electrolyte solution (NaCl or $CaCl_2$) and velocity were kept constant in a given transport experiment. The steady-state Darcy velocity of approximately 0.7 cm/min was applied to the column in an up-flow mode using a peristaltic pump. The transport experiment was conducted using the following sequence. The packed column was preconditioned with around 50 pore volumes (PV) of a selected background electrolyte solution. A D_2O tracer pulse (100 mL) was injected into the column followed by at least 5 PV of the background solution. A 100 mL pulse of the GO suspension was injected into the column, followed by flushing with several PV of the particle-free background solution until the effluent concentration was <0.5% of the input concentration (Phase I). The influent GO suspension was continuously mixed with a magnetic stirrer during GO injection. The column effluent was collected continuously in glass tubes using a fraction collector with 4 mL for each sample. Effluent concentrations of the tracer were quantified by a high-performance liquid chromatography (D-7000 HPLC, High-Technologies Corporation, Japan) with a refractive index detector, whereas the GO concentration was determined using the UV–Vis spectrophotometer. Tracer and GO breakthrough curves (BTCs) were obtained from these effluent concentrations. After recovery of the BTCs, the porous medium in the packed column was carefully excavated in 1 cm increments (12 layers in total) and placed in DI water to release and resuspend GO for concentration measurements. The GO retention profile (RP) was subsequently determined from this information and the measured dry mass of sand in each increment.

2.3.2. Release experiments

Additional experiments were conducted to study the influence of IS reduction and cation exchange on the release of GO following the recovery of the BTC. Determination of the GO BTC followed the same protocol as for the transport experiment (Phase I). After recovery of the GO BTC in various NaCl and $CaCl_2$ solutions, different solution chemistry elution sequences were applied to deduce the effects of the IS reduction and cation exchange on the release of the retained GO. The GO release by the IS reduction was studied by flushing columns with DI water (Phase II). This is the only release phase that was considered when GO was retained in the presence of the NaCl solution. Conversely, when GO was retained in the presence of $CaCl_2$ (Phase I) then a series of solution chemistry elution steps was employed in the release phase, namely: DI water (Phase II); NaCl at the same IS as in the retention experiment (Phase III); DI water (Phase IV); 100 mM NaCl (Phase V); and DI water (Phase VI). After completion of the release experiment, the GO RP was determined following the same protocol as for the transport experiments.

2.4. Interaction energy calculations

Interaction energy calculations were conducted to better understand mechanisms contributing to GO aggregation, retention, and release under various solution chemistry conditions. In this work, the GO geometry, GO orientation, surface roughness, and nanoscale chemical heterogeneity were considered for interaction energy calculations. Section S2 of the Supporting information (SI) provides details pertaining to these calculations. The dimensionless depths of the primary (Φ_{1min}) and secondary (Φ_{2min}) minima, and the energy barrier height (Φ_{bar}) were obtained by analyzing the interaction energy profiles.

2.5. Mathematical modeling

Numerical simulations of GO transport experiments were conducted using HYDRUS-1D (Šimůnek et al., 2016) to quantify mechanisms of retention (Phase I), blocking or ripening (Phase I), and transient release (Phases II–VI). Section S3 of the Supporting information describes the modeling approach in detail. Values of the Darcy velocity (q), porosity (θ), bulk density (ρ), and dispersivity (λ) were determined from available experimental information and the D_2O tracer. Other model parameters were determined by optimization to GO BTCs, RPs, and/or release pulses using the nonlinear least squares fitting routine in HYDRUS-1D (Šimůnek et al., 2016). The retention rate coefficient (k_{sw}) was optimized during Phase I, along with the normalized maximum solid

phase concentration of deposited GO (S_{max}/C_o) for blocking or the empirical parameter (γ) for ripening. The transient release rate coefficient (k_{rs}) and the equilibrium release fraction (F_{eq}) were optimized during Phases II–VI, whereas the fraction of retained GO that was not released (f_{nr}) was determined from mass balance calculations.

3. Results and discussion

3.1. GO-sand and GO-GO interactions

Table S1 presents a summary of zeta potentials and hydrodynamic diameters (d_p) for various NaCl (1 to 200 mM) and $CaCl_2$ (0.10 to 1.67 mM) solution chemistry conditions considered in this work. This information on zeta potential and hydrodynamic diameter is also shown as a function of the solution chemistry in Figs. S1 and S2, respectively. The zeta potential increased from −49.7 to −27.2 mV for sand as the IS increased from 1 to 200 mM NaCl due to the compression of the double layer thickness and charge screening (Torkzaban et al., 2010). Similarly, the zeta potential of GO increased from −29.3 to −18.7 mV over the IS range of 0 to 200 mM NaCl when the GO concentration was 10 mg L^{-1}. Although the change in GO zeta potentials was rather small, it was sufficient to significantly alter values of d_p, which increased from around 600 nm to almost 2000 nm (Fig. S2a).

Small changes in the IS produced much larger changes in zeta potential and d_p for $CaCl_2$ than NaCl (Table S1, Figs. S1 and S2). In particular, the value of d_p increased from 600 to 8000 nm as the $CaCl_2$ concentration increased from 0.10 to 1.67 mM. In addition to compression of the double layer and charge screening, adsorbed Ca^{2+} ions can also produce nanoscale chemical heterogeneity due to charge neutralization or reversal (Grosberg et al., 2002; Roy and Dzombak, 1996) and/or cation bridging (Torkzaban et al., 2012). These factors can explain the enhanced sensitivity of d_p to $CaCl_2$ than NaCl.

Interaction energy parameters provide additional insight into factors that contribute to GO retention and aggregation. Table S2 summarizes interaction energy parameters for GO with sand or another GO particle for all solution chemistries when GO is oriented parallel to the interacting surface. The energy barrier height (Φ_{bar}) and the magnitude of the secondary minimum (Φ_{2min}) tend to increase with increasing IS. Note that the probability of GO interaction in a primary minimum (Φ_{1min}) rapidly goes to 0 as Φ_{bar} becomes greater than around 5.7 (Bradford et al., 2015). The GO aggregation is therefore only predicted to occur in a strong Φ_{1min} under low IS conditions (1 mM NaCl and ≤ 0.4 mM $CaCl_2$) because Φ_{bar} is smaller than 5.7, whereas no aggregation is predicted for a higher IS because Φ_{2min} is zero. This behavior is clearly not consistent with the experimental observations (Figs. S1 and S2). GO interaction with sand is predicted to be dominated by Φ_{2min} with an increasing IS. Similar conclusions have been reported by other investigators for the parallel orientation of GO (Wu et al., 2013b). However, these calculations do not consider the potentially significant influence of other GO orientations, GO thickness, nanoscale roughness, and chemical heterogeneity on GO interactions that will be discussed below.

Table S3 shows an illustrative example of the influence of the GO thickness (i.e., the GO thickness of 1 or 10 nm) and orientation (parallel and perpendicular) on GO-GO and GO-sand interactions when the IS = 20 mM NaCl. Thicker (layered) GO particles increased the magnitudes of Φ_{bar} and Φ_{2min}, and the importance of secondary minimum interactions. Conversely, the perpendicular orientation of GO particles with interacting surfaces drastically decreases the magnitudes of Φ_{bar}, Φ_{2min}, and Φ_{1min} in comparison to the parallel orientation, and therefore increases the probability of primary in comparison to secondary minimum interactions.

The role of nanoscale roughness on interaction energy calculations was subsequently investigated. Nanoscale roughness is ubiquitous on sand surfaces (Konopinski et al., 2012; Shellenberger and Logan, 2002; Shen et al., 2011). Table S4 presents interaction energy parameters for GO with sand or another GO particle for all solution chemistries when GO is oriented perpendicular to the interacting surface that has a nanoscale roughness height of 30 nm and a fraction of 0.05 on the sand surface. Table S5 shows similar calculations when the nanoscale roughness of height of 30 nm and a fraction of 0.05 occurs on both surfaces. A perpendicular orientation of GO in conjunction with small amounts of nanoscale roughness drastically decreases the magnitudes of Φ_{bar}, Φ_{2min}, and Φ_{1min} and creates primary minimum interactions under all solution chemistry conditions. However, Φ_{1min} is very shallow and susceptible to diffusive and/or hydrodynamic release only when roughness occurs on both surfaces. It should be mentioned that the perpendicular orientation is the optimum scenario for primary minimum interactions, but that nanoscale roughness will similarly influence Φ_{bar}, Φ_{2min}, and Φ_{1min} in the parallel orientation. Furthermore, adsorbed Ca^{2+} ions to surfaces can produce nanoscale chemical heterogeneity due to charge neutralization or reversal (Grosberg et al., 2002; Roy and Dzombak, 1996) and/or cation bridging (Torkzaban et al., 2012). Such nanoscale charge heterogeneity has been demonstrated to produce primary minimum interactions by lowering Φ_{bar} and increasing the depth of Φ_{1min} on a relatively smooth surface, but its relative importance decreases on surfaces with small amounts of nanoscale roughness (Bradford et al., 2017; Bradford et al., 2018).

The above information indicates that GO retention and aggregation will be a strong function of the solution IS, the GO orientation and thickness, the nanoscale roughness on the sand and GO, and the amount of chemical heterogeneity induced by the presence of Ca^{2+} ions. Variability in these parameters is expected to produce different strengths and modes of interaction (e.g., a secondary in comparison to the primary minimum) that contribute to GO aggregation, retention, and release. Primary minimum interactions due to nanoscale roughness and perpendicular orientation are expected to be more important at a lower IS and for $CaCl_2$ experiments. Conversely, both primary and secondary minimum interactions are expected for the NaCl experiments, with secondary minimum playing a larger role at a higher IS.

3.2. Aggregation of GO

The GO aggregation behavior was investigated over a 50 min period under different IS and compositions (NaCl and $CaCl_2$ solutions). Fig. 1a and b present values of d_p as a function of the concentration of NaCl and $CaCl_2$ solutions, respectively. GO suspensions were relatively stable only under 1 mM, 10 mM, and 20 mM NaCl, and 0.10 and 0.20 mM $CaCl_2$ conditions. Conversely, values of d_p gradually increased with time and exhibited fluctuations when concentrations were >20 mM NaCl or 0.2 mM $CaCl_2$ and became larger with increasing IS and in the presence of $CaCl_2$ than NaCl.

The GO aggregation behavior presented in Fig. 1a and b was described with the attachment efficiency (α) (Eq. (S3)). The attachment efficiency as a function of the concentration of NaCl and $CaCl_2$ is also presented graphically in Fig. S3. It was determined by normalizing the aggregation rate constant (k_a) (Eq. (S2)) obtained in a specific background solution chemistry to the rate constant that was the most favorable for aggregation ($k_{a,\ fast}$) (Chen and Elimelech, 2006; Wu et al., 2013b). Variations in d_p with the solution chemistry in Fig. 1a and b can be attributed to differences in the attachment efficiency, which increases with the IS at a lower concentration for $CaCl_2$ than NaCl (Fig. S3). These trends can be explained by interaction energy parameters shown in Tables S2–S5. In particular, the potential for secondary and primary minimum interactions increases with increasing IS due to compression of the double layer and charge screening. Secondary minimum interactions are expected to be more pronounced for parallel GO configurations, whereas strong primary minimum interactions may sometimes occur for perpendicular GO configurations. These contributions occur at a lower IS in the presence of Ca^{2+} ions which induce nanoscale chemical heterogeneity (e.g., local charge neutralization or reversal, and/or cation bridging).

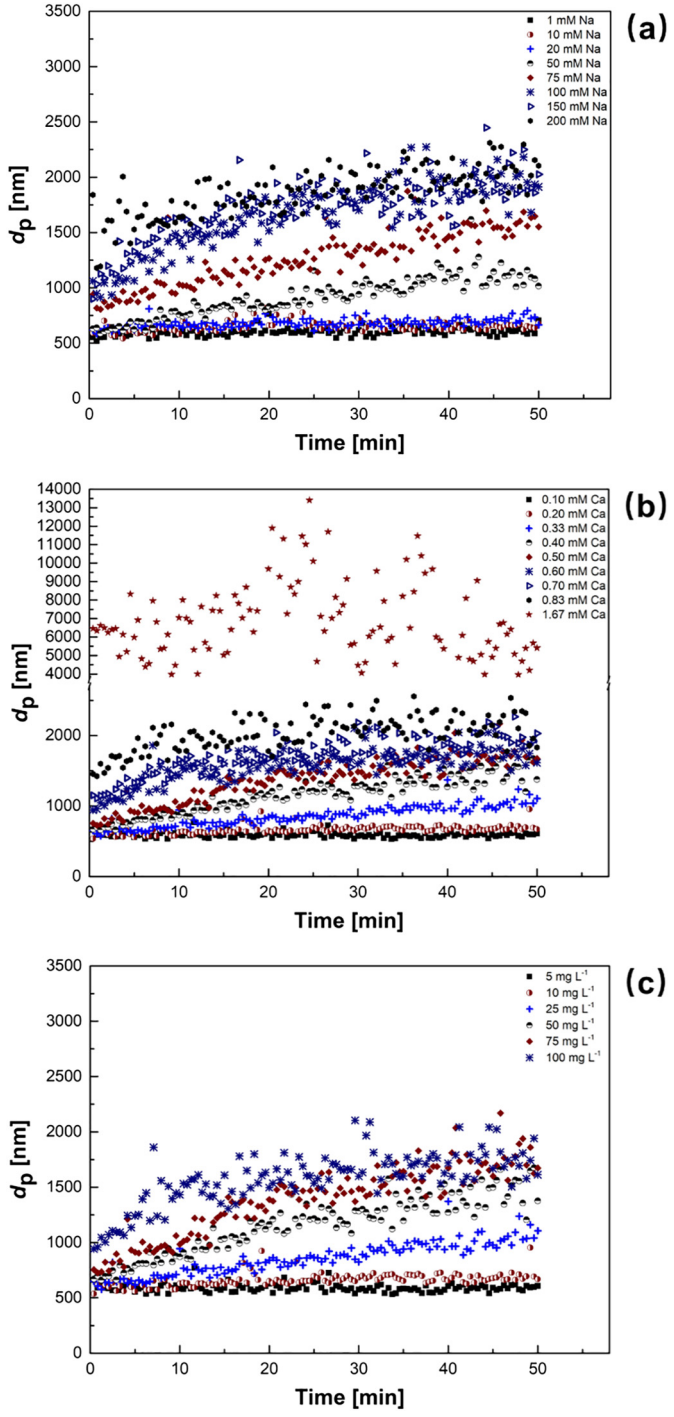

Fig. 1. Aggregation of graphene oxide over 50 min as a function of the ionic strength in NaCl (a), $CaCl_2$ (b), and initial GO suspension concentration in 50 mM NaCl solution (c).

Additional experiments were conducted to investigate the influence of the initial GO suspension concentration on the aggregation behavior. Fig. 1c presents values of d_p over a 50 min period as a function of the initial GO suspension concentration in the 50 mM NaCl solution. The value of d_p increases with time and the initial GO suspension concentration. Fig. 1c indicates that aggregation rapidly increased with the initial GO suspension concentration. In particular, the average distance between GO particles decreases with increasing suspension concentration and this produces an increased frequency of GO collisions. Consequently, this concentration dependency of aggregation occurs because of differences in the aggregation rate (Baalousha, 2009; Lee, 1983).

3.3. Transport, retention, and release of GO

This section discusses BTCs and RPs for GO under different IS, cation types, influent GO concentrations, and sand grain sizes. The BTCs are plotted as normalized effluent concentrations (C/C_o) versus pore volumes. The RPs are plotted as normalized solid phase concentrations (S/C_o) as a function of the distance from the column inlet. Some of the figures which present BTCs also include release curves (RCs) under transient solution chemistry conditions. Experimental conditions and the mass balance for each column experiment are summarized in Table 1. Simulated BTCs, RPs, and RCs are also shown in the figures. Table 2 presents a summary of the fitted model parameters as well as statistical measures of the goodness of fit.

3.3.1. Ionic strength

Fig. 2 presents observed and simulated BTCs and RCs for GO when using 1090 μm quartz sand, $C_o = 10$ mg L^{-1}, and the IS equal to 1, 20, and 100 mM NaCl during Phase I. An increase in the solution IS led to a significant decrease of GO mobility (the effluent mass balance, M_{eff}, in Table 1) and enhanced retention (k_{sw} in Table 2) due to the compression of the double layer thickness and charge screening (Dong et al., 2016; Liu et al., 2013; Wang et al., 2017a; Wang et al., 2018; Xia et al., 2015). Interaction energy parameters reveal that increasing the solution IS increases the depth of the secondary minimum (Table S2) and the frequency of primary minimum interactions that may sometimes occur depending on local scale variations in sand surface roughness and the GO orientation (Tables S4 and S5). In addition, the value of d_p for GO also increased with the solution IS (Fig. 1) and filtration theory indicates that this will alter the rate of mass transfer to the sand surface; e.g., the minimum in the mass transfer is expected to occur around d_p = 1500 nm (Messina et al., 2015).

Table 1
Experimental parameters and the mass recoveries of graphene oxide transport and release experiments.

	d_{50}	C_o	Cation	Recovery, %					
	μm	mg L^{-1}	mM	M_I	M_{II}	M_{III}	M_{IV}	M_V	M_{VI}
Fig. 2	1090	10	1 Na^+	95.6	1.2				
	1090	10	20 Na^+	76.3	3.9				
	1090	10	100 Na^+	24.8	24.4				
Fig. 3	1090	10	0.33 Ca^{2+}	91.2	0.6	1.1	3.8	1.6	8.1
	1090	10	0.40 Ca^{2+}	28.7	0.1	0.0	0.1	0.5	11.2
	1090	10	0.83 Ca^{2+}	11.8	1.6	2.1	2.3	3.0	9.7
	1090	10	1.67 Ca^{2+}	0.7	0.5	0.1	0.4	0.0	2.5
Fig. S5	1090	10	100 Na^+	16.3	11.9				

	d_{50}	C_o	Cation	Recovery, %		
	μm	mg L^{-1}	mM	M_{eff}	M_{sand}	M_{total}
Fig. 4	1090	5	50 Na^+	68.7	33.5	101.2
	1090	10	50 Na^+	65.2	36.9	102.1
	1090	50	50 Na^+	38.4	59.8	98.2
	1090	100	50 Na^+	29.7	67.6	97.3
Fig. 5ab	1090	10	50 Na^+	65.2	36.9	102.1
	519	10	50 Na^+	50.7	48.8	99.5
	330	10	50 Na^+	39.9	65.1	105.0
Fig. 5cd	1090	100	50 Na^+	29.7	67.6	97.3
	519	100	50 Na^+	19.0	76.8	95.8
	330	100	50 Na^+	12.5	86.1	98.6
Fig. S4	1090	10	1 Na^+	96.0	8.6	104.6
	1090	10	50 Na^+	65.2	36.9	102.1
	1090	10	100 Na^+	20.7	86.1	106.8

Fig. 2: release of graphene oxide (GO) by ionic strength reduction; Fig. 3: release of retained GO by cation exchange and ionic strength reduction; Fig. 4: concentration effect; Fig. 5ab: grain size effect ($C_o = 10$ mg L^{-1}); Fig. 5cd: grain size effect ($C_o = 100$ mg L^{-1}); Fig. S4: ionic strength effect; Fig. S5: GO release was initiated by reversing the flow direction; C_o, input concentration of GO; M_I – M_{VI} are the mass percentages recovered from Phase I–VI in release experiments; M_{eff}, M_{sand}, and M_{total} are mass percentages recovered from effluent, sand, and total in transport experiments, respectively.

Table 2
Fitted parameter values of graphene oxide retention (S_{max}/C_o, k_{sw}) and release (F_{eq}, k_{rs}, and f_{nr}) experiments.

	d_{50}	C_o	Cation	S_{max}/C_o,	k_{sw},	F_{eq},	k_{rs},	R^2
	μm	mg L^{-1}	mM	cm^3 g^{-1}	min^{-1}		min^{-1}	
Fig. 2	1090	10	1 Na^+	0.043	0.031	0.101	0.080	0.999
	1090	10	20 Na^+	0.216	0.114	0.141	0.820	0.997
	1090	10	100 Na^+	1.493	0.162	0.455	0.393	0.915
Fig. 3	1090	10	0.33 Ca^{2+}	0.076	0.046		0.207	0.958
	1090	10	0.40 Ca^{2+}	0.442	0.096		0.566	0.651
	1090	10	0.83 Ca^{2+}	0.334	0.191		0.159	0.808
	1090	10	1.67 Ca^{2+}	148.640	3.633		0.116	0.985
Fig. 4	1090	5	50 Na^+	0.619	0.066			0.977
	1090	10	50 Na^+	0.444	0.068			0.979
	1090	50	50 Na^+	1398.200	0.145			0.892
	1090	100	50 Na^+	0.353	0.087			0.962
Fig. 5ab	1090	10	50 Na^+	0.444	0.068			0.979
	519	10	50 Na^+	0.552	0.167			0.956
	330	10	50 Na^+	0.649	0.269			0.937
Fig. 5cd	1090	100	50 Na^+	2.319	0.186			0.891
	519	100	50 Na^+	162,500.000	0.219			0.850
	330	100	50 Na^+	7.383	0.246			0.844
Fig. S4	1090	10	1 Na^+	0.045	0.052			0.998
	1090	10	50 Na^+	0.444	0.068			0.979
	1090	10	100 Na^+	2.370	0.187			0.780

	d_{50}	C_o	Cation	f_{nr} (II)	f_{nr} (III)	f_{nr} (IV)	f_{nr} (V)	f_{nr} (VI)
	μm	mg L^{-1}	mM					
Fig. 2	1090	10	1 Na^+	0.84				
	1090	10	20 Na^+	0.84				
	1090	10	100 Na^+	0.68				
Fig. 3	1090	10	0.33 Ca^{2+}	0.93	0.81	0.38	0.19	0.00
	1090	10	0.40 Ca^{2+}	1	1	1	0.99	0.83
	1090	10	0.83 Ca^{2+}	0.98	0.96	0.93	0.90	0.79
	1090	10	1.67 Ca^{2+}	0.99	0.99	0.99	0.99	0.96

S_{max}/C_o, the normalized maximum solid phase concentration of deposited nanoparticles; k_{sw}, the retention rate coefficient; F_{eq}, equilibrium release fraction; k_{rs}, the transient release rate coefficient; f_{nr}, the fraction of retained GO that is not released in Phases II to VI; R^2, Pearson's correlation coefficient.

Blocking was observed and captured by the model when the IS was 1 and 20 mM NaCl. Fitted values of S_{max}/C_o (Table 2) increase with IS, indicating that more of the solid surface area contributed to GO retention. Conversely, continued injection of GO produced a slight decrease in the effluent concentration of GO when the IS was 100 mM. This behavior was accurately captured (Table 2) by the ripening model (Eq. (S19)), although aggregation of GO may also produce this result due to a decrease in the total number of GO particles (Bradford and Leij, 2018). Table 1 and Fig. 1 clearly demonstrate that GO-GO interactions and aggregation, respectively, occurred in the aqueous phase when the IS = 100 mM. However, aggregation and ripening are related processes that reflect GO-GO interactions in the aqueous phase and the solid phase, respectively. It was not possible to separate these effects from the collected information, but it is logical to anticipate that both aggregation and ripening may be occurring simultaneously.

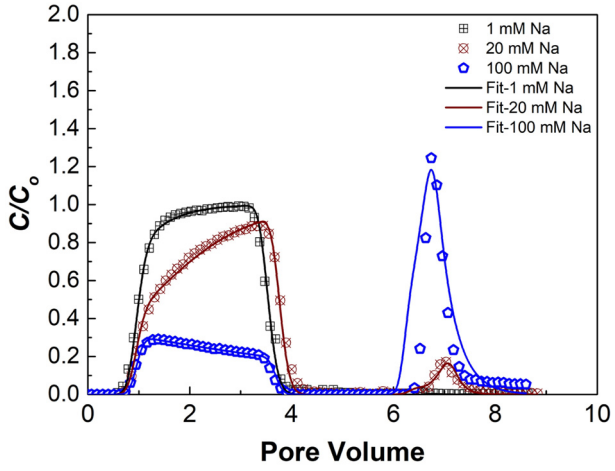

Fig. 2. Transport, retention and release behavior of graphene oxide in quartz sand. Retention occurred at an ionic strength of 1, 20, and 100 mM NaCl, respectively, whereas release was initiated by eluting with DI water. Other experimental conditions were the same: input concentration, 10 mg L^{-1}; grain size, 1090 μm; Darcy velocity, 0.7 cm/min.

Fig. 2 also shows observed and simulated RCs when the IS during Phase I (1, 20, and 100 mM) was reduced to DI water during Phase II. The effluent mass of GO during Phase II was equal to 1.2, 3.9, and 24.4% when the Phase I IS equaled 1, 20, and 100 mM NaCl, respectively (Table 1). This trend of increasing effluent mass with the IS during Phase I reflects differences in the amount of GO retention. Around 16 to 32% of the retained GO was released when the IS was decreased to DI water. The GO release with IS reduction was adequately modeled (Table 2) using a release model that considered both equilibrium and kinetic sites (Eqs. S20–S22). GO release with IS reduction may occur due to either elimination of the secondary minimum, and/or a decrease in the energy barrier to detachment from a primary minimum to less than around 5.7 on a nanoscale rough surface (Shen et al., 2018). Release from a secondary minimum with IS reduction is expected to approach equilibrium conditions (F_{eq}), whereas release from a primary minimum is expected to be a slower diffusion-controlled process (k_{rs} would become small for deeper minima). Fitted values of F_{eq} and k_{rs} tended to increase and decrease, respectively, with an increase in IS during Phase I. This increase in F_{eq} with IS likely reflects an increasing contribution of secondary minimum interactions (Table S2). However, the release from both primary and secondary minima apparently occurred during Phase II due to differences in the GO orientation with the surface and the roughness conditions which produced different interaction strengths (Tables S2–S5).

Fig. S4a presents observed and simulated GO BTCs when the IS = 1, 50, and 100 mM NaCl and other conditions were the same as in Fig. 2.

Tables 1 and 2 provide mass balance results and model parameters for these experiments. The BTCs and trends with IS were fully consistent with those shown in Fig. 2 and demonstrated the reproducibility of the results. Fig. S4b presents observed and simulated RPs for GO following completion of Phase I when the IS = 1, 50, and 100 mM NaCl. Consistent with the BTC information (Fig. 2), the retained mass of GO in the sand increased with IS (Table 1). The RPs for the IS = 1 and 50 mM NaCl were generally well described by the blocking model (Fig. S4b and Table 2). Similarly, the ripening model provided a reasonable description of the IS = 100 mM data (Fig. S4b and Table 2), and consistent with experimental observations exhibited greater retention near the sand surface than for the low IS conditions. Table 1 indicates that nearly all of the retained GOs were recovered when determining the RP (the total recovered mass ranged from 102.1 to 106.8%). In contrast, only 16 to 32% of the retained GO were recovered with the RC in Fig. 2 during Phase II. This observation indicates that most of the retained GO following IS reduction were associated with a shallow primary minimum on a rough sand surface (Tables S4 and S5), and that level arms from microscopic roughness and grain-grain contacts played an important role in the GO retention (Torkzaban and Bradford, 2016; Zhang et al., 2016); e.g., the lever arms are constant during Phases I and II, whereas they randomly vary during determination of the RP. An additional experiment was conducted to further demonstrate the role of pore structure on the GO retention. Fig. S5 shows a replicate of the 100 mM experiment. In this case, the GO release was initiated by reversing the flow direction and keeping the IS = 100 mM. A very large release pulse was observed when the flow was reversed that accounted for 11.9% of the injected GO mass, which confirms the importance of surface straining processes for GO.

3.3.2. Cation type and exchange

Additional experiments were conducted to study the influence of a multivalent cation and cation exchange on GO transport and release, respectively. Fig. 3a presents observed and simulated BTCs for GO in the presence of 0.33, 0.40, 0.83, and 1.67 mM $CaCl_2$ when using 1090 μm quartz sand, and C_o = 10 mg L^{-1}. Similar to NaCl (Fig. 2), increasing the $CaCl_2$ concentration produced an increase in the GO retention due to the compression of the double layer thickness and charge screening. However, $CaCl_2$ had a much larger influence on the GO retention than NaCl (Fig. 2), even though its IS was much lower (<5 mM). This can be explained by the greater influence of Ca^{2+} than Na^+ on the zeta potentials of the sand and GO (Fig. S1), as well as the interaction energies (Tables S2–S5). Furthermore, Ca^{2+} also enhances aggregation (Fig. 1) and retention (Figs. 2 and 3a) in comparison to Na^+ due to cation bridging and/or charge neutralization or reversals, which reflect a form of nanoscale chemical heterogeneity (Grosberg et al., 2002; Roy and Dzombak, 1996; Torkzaban et al., 2012). In comparison to the NaCl experiments (Fig. 2), the retention of GO in the presence of $CaCl_2$ is expected to be more dependent on primary minimum interactions (e.g., the depth of the secondary minimum is much smaller at the lower IS < 5 mM) which may occur on rough surfaces and in the presence of nanoscale chemical heterogeneity (Tables S4 and S5), and on surface straining processes because of larger aggregate sizes (Fig. 1).

The blocking (Eq. (S18)) or ripening (Eq. (S19)) model accurately described the measured GO BTCs (Table 2). Blocking was only observed in Fig. 3a when the $CaCl_2$ concentration was 0.33 mM. Conversely, the ripening behavior was observed when the $CaCl_2$ concentration was 0.40 and 0.83 mM. Furthermore, almost no breakthrough of GO occurred when the $CaCl_2$ concentration was 1.67 mM. This ripening and complete retention behavior reflect the potential for increasing GO-GO interactions in the liquid phase (Fig. 1 and S3) and on the solid phase with increasing $CaCl_2$ concentrations.

The RCs shown in Fig. 3a provide additional insight into the mechanisms of GO retention and release. For example, injection of DI water following completion of Phase I (recovery of the BTC), produced a very minor amount of GO release (<1.6%) and this further confirms

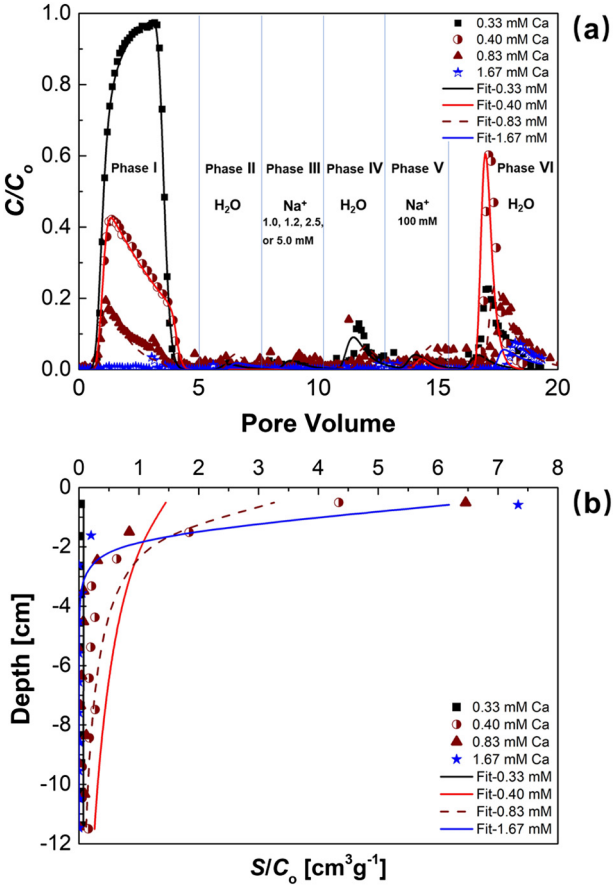

Fig. 3. (a) Retention and release behavior of graphene in quartz sand. Retention (Phase I) occurred at a $CaCl_2$ concentration of 0.33, 0.40, 0.83 and 1.67 mM (IS = 1.0 1.2, 2.5, and 5.0 mM) respectively, whereas release was initiated by eluting with DI water (Phases II, IV, and VI) and cation exchange (Phases III and V) as summarized in Table 1. (b) Retention profiles after completion of release experiments. Other experimental conditions were the same: input concentration, 10 mg L^{-1}; grain size, 1090 μm; Darcy velocity, 0.7 cm/min.

the lack of secondary and the dominance of primary minimum interactions (Tables S2–S5). Two sequences of cation exchange and expansion of the double layer were subsequently initiated by injecting various strengths of the NaCl solution followed by DI water, respectively. The exchange of Ca^{2+} on the solid phase increases with increasing injected NaCl concentrations (Bradford and Kim, 2010). Very little GO release occurred during the injection of the NaCl (1 to 100 mM) solutions (<3%). However, much larger amounts of the GO release occurred following cation exchange in the presence of DI water when the double layer was expanded (as high as 11.2%). This GO release depended on the $CaCl_2$ concentration during Phase I and the NaCl concentration during the cation exchange phase; e.g., higher $CaCl_2$ concentrations tended to produce less GO release and higher NaCl concentrations enhanced release. These observations indicate that the strength of the primary minimum interactions, caused in part by Ca^{2+}adsorption, can sometimes be reversed by cation exchange and expansion of the double layer. Consistent with primary minimum interactions, the release model indicates a slower release behavior for GO in the presence of $CaCl_2$ than in NaCl (Fig. 2) that was adequately described using the one-site kinetic release model (Eqs. S20–S22 with F_{eq} = 0).

Observed and simulated GO RPs in the $CaCl_2$ experiments are shown in Fig. 3b following completion of Phase VI. Only limited GO retention occurred when the $CaCl_2$ concentration during Phase I equaled 0.33 mM, and the RP distribution with depth was nearly uniform. In contrast, the vast majority of the GO retention occurred near the column inlet when the $CaCl_2$ during Phase I equaled 0.40, 0.83, and 1.67 mM.

This hyper-exponential retention was only partially captured by the ripening model (Eq. (S19)) (Table 2), and this non-exponential behavior reflects the combined influence of enhanced aggregation (Fig. 1) and surface straining (Fig. S5) in the presence of $CaCl_2$ (Lanphere et al., 2014). The GO mass balance was nearly complete after recovery of the BTCs, RCs, and RPs (Table 1). Similar to the NaCl experiments (Fig. 2), this indicates that GO was interacting in the presence of a shallow primary minimum and/or the significant influence of lever arms on GO retention (Torkzaban and Bradford, 2016; Zhang et al., 2016).

3.3.3. Input concentration

Column experiments were conducted to explore the influence of C_o on GO transport and retention. Fig. 4 presents observed and simulated BTCs and RPs for C_o = 5, 10, 50, and 100 mg L^{-1} when the IS = 50 mM NaCl and the sand size was 1090 μm. Some evidence of blocking is apparent in the BTCs when C_o = 5, 10, and 100 mg L^{-1}; e.g., an increasing effluent concentration during GO injection. Furthermore, the blocking model provided a satisfactory description of the BTCs (Table 2), although the model under-predicted the RP concentration near the inlet with increasing C_o. Blocking is also expected to be a function of C_o. In particular, larger values of C_o should fill up a fixed number of retention sites more rapidly and produce a higher effluent concentration when a stable, monodispersed suspension is considered (e.g., Leij et al., 2015). Conversely to this expected behavior for blocking, Fig. 4 shows that the GO effluent mass decreased with increasing C_o (Table 1). This observation was therefore attributed to the faster aggregation and larger aggregate sizes that occur with increasing C_o (Fig. 1c). An increase in the aggregate size will alter the rate of mass transfer to the solid surface (Messina et al., 2015), increase the energy barrier and the depth of the secondary minimum (Shen et al., 2007), and produce more surface straining (Lanphere et al., 2013). These factors likely explain the deviations between blocking model for experimental RPs at higher values of C_o.

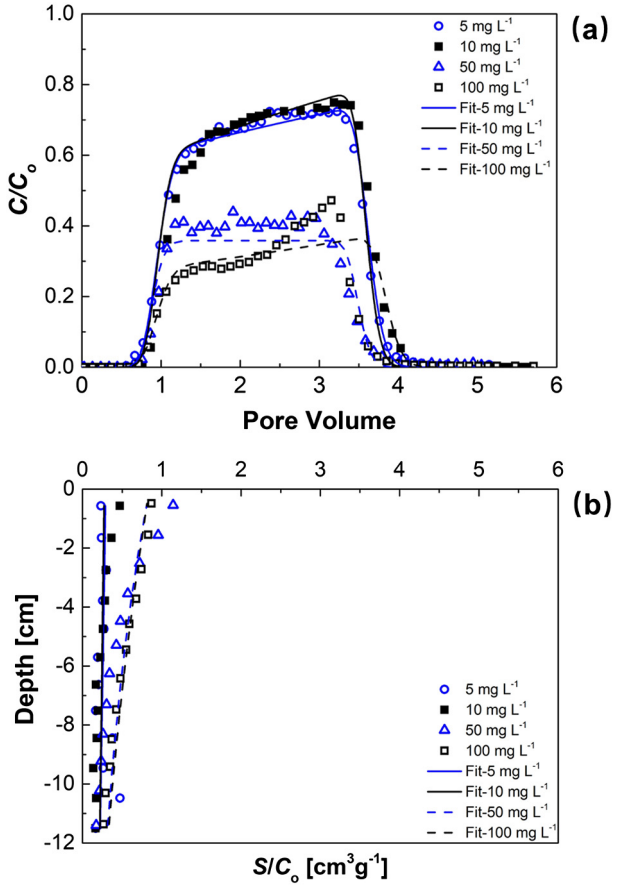

Fig. 4. Effect of input concentration on the transport and retention of graphene oxide (GO) in quartz sand: breakthrough curves (a) and retention profiles (b) of GO under input concentrations of 5, 10, 50, and 100 mg L^{-1}, respectively. Other experimental conditions were the same: electrolyte, 50 mM NaCl; grain size, 1090 μm; Darcy velocity, 0.7 cm/min.

3.3.4. Grain size

A sand grain size is another important factor that influences GO transport and retention due to its influence on GO mass transfer to the solid and pore structure geometry. Fig. 5a and b show observed and predicted BTCs and RPs, respectively, for GO when the median sand size equaled 330, 519, and 1090 μm, the IS = 50 mM NaCl, and C_o was 10 mg L^{-1}. Fig. 5c and d show similar information when C_o = 100 mg L^{-1}. The aggregation rate is much slower and the aggregate size is smaller when C_o is 10 than 100 mg L^{-1} (Fig. 1c). Differences in BTCs and RPs shown in Fig. 5a and b are therefore mainly due to the influence of the GO mass transfer. In particular, the filtration theory predicts that the mass transfer rate to the solid surface increases with a decrease in the median grain size and this produces a higher value of k_{sw} (Table 2) and more retention (Table 1). The fitted value of S_{max}/C_o also increases with decreasing grain size (Table 2), and this suggests the presence of more retention sites. The nearly complete mass balance from BTCs and RPs (Table 1) indicates that retained GO was weakly associated with the solid phase either due to shallow secondary or primary minima, and alteration of the lever arms during recovery of the RPs liberated them.

There are similarities and differences in the GO BTCs and RPs in various sands when C_o equals 10 (Fig. 5ab) and 100 (Fig. 5cd) mg L^{-1}. Similar to Fig. 5ab, Fig. 5cd show an increase in retention with a decrease in the median sand size due to differences in the GO mass transfer rate. In contrast to Fig. 5ab, Fig. 5cd show a greater amount of retention and more hyper-exponential RPs when C_o = 100 mg L^{-1}. Similar to Fig. 4 these observations were attributed to an increase in the aggregation rate and size with an increase in C_o (Fig. 1c). It is interesting to note that these effects of C_o did not have a large influence on the RP shape for the largest 1090 μm median grain size, but had a pronounced influence on the RP shape for smaller 519 and 330 μm grain sizes. This clearly demonstrates that hyper-exponential RPs were more pronounced in smaller sands and at a higher C_o. Both of these factors are consistent with physical retention mechanisms, such as surface straining, in producing hyper-exponential RPs.

4. Conclusions

The aggregation, retention, and release behaviors of GO were investigated under different physicochemical conditions (IS, cation type, C_o, and d_{50}). Results indicate that greater GO transport occurred at a lower IS, monovalent in comparison to divalent cations, lower C_o, and in the coarser textured sand. Furthermore, reversible GO retention occurred with decreases in IS as a result of the expansion of the double layer and/or cation exchange. Novel interaction energy calculations indicated that GO retention and aggregation would be a strong function of the solution IS, the GO orientation, the roughness of the sand and GO, and the amount of chemical heterogeneity induced by the presence of adsorbed multivalent cations. Secondary minimum interactions increased with an IS, whereas primary minimum interactions occurred at a low IS, especially on rough surfaces and for a perpendicular orientation of GO with the surface. Aggregation and retention of GO were much stronger in the presence of $CaCl_2$ at a low IS than NaCl at a higher IS, due to cation bridging and/or charge neutralization or reversals which reflect a form of nanoscale chemical heterogeneity. Only a fraction of GO was released when the IS was reduced to DI water. This released fraction decreased when GO was initially deposited in the presence of $CaCl_2$ but could be enhanced by later cation exchange (Na^+ displaced Ca^{2+} on the solid). This observation indicates that the primary minimum also contributed to GO retention and release and that cation exchange and the IS reduction could alter the strength of this interaction. However, the

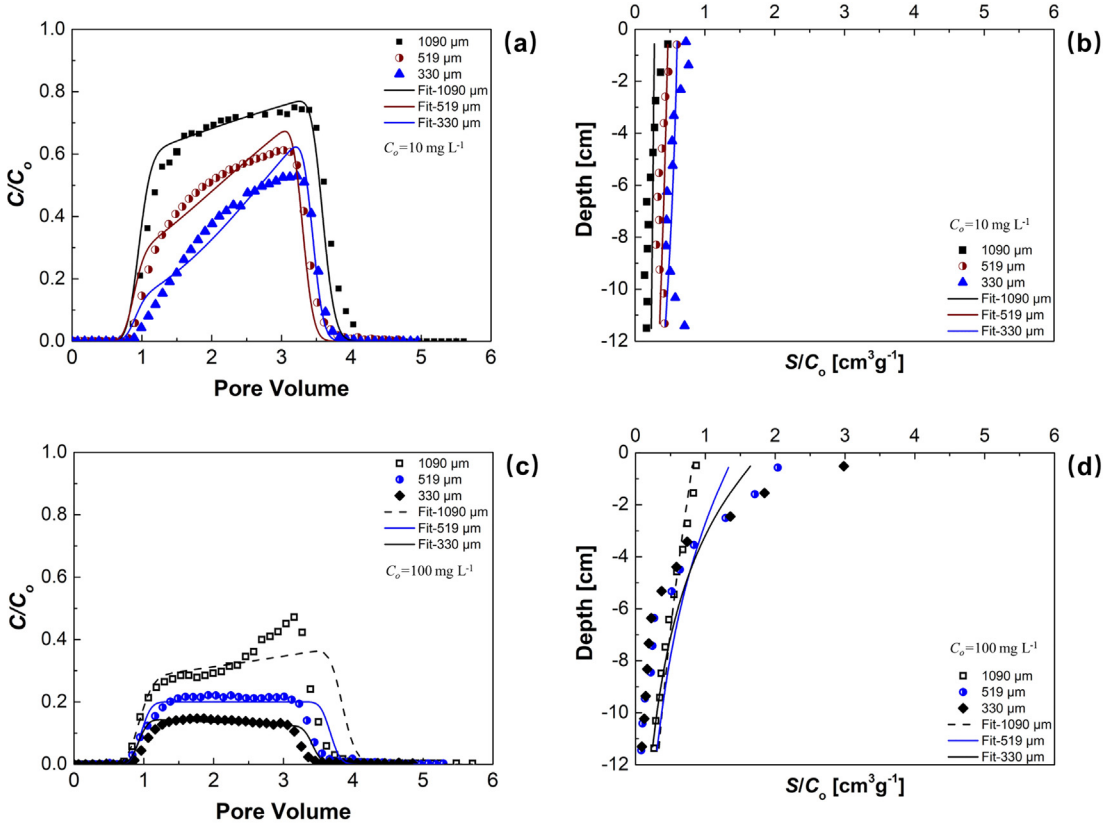

Fig. 5. Effect of grain size on the transport and retention of graphene oxide (GO) in quartz sand: breakthrough curves and retention profiles of GO under input concentrations of 10 mg L^{-1} (ab) and 100 mg L^{-1}(cd). Other experimental conditions were the same: electrolyte, 50 mM NaCl; Darcy velocity, 0.7 cm/min.

GO mass was completely recovered in the BTCs, RCs, and RPs. These findings indicate that retained GO was mainly captured in a shallow primary minimum on a rough sand surface and that level arms from microscopic roughness and grain-grain contacts played an important role in GO retention, e.g., the level arms acting on retained GO randomly varied when the sand was excavated from the column and then placed in DI water. In addition, the coupled effects of aggregation and straining were shown to be influenced by C_o and d_{50}, and these processes also altered blocking, ripening, and RP shapes. The main features of these observations were well described by a mathematical model that accounted for blocking, ripening, and release of GO during transient solution chemistry conditions. This information is needed to better understand and predict the interactions, retention, and release of colloids/nanoparticles, especially particles with plate structure, in natural and engineering applications.

Acknowledgments

This research was funded by the National Natural Science Foundation of China (Grant No. 21507015; 170101), Guangxi Natural Science Foundation, China (Grant No. 2015GXNSFCA139015; 2017GXNSFBA198076). The authors would like to acknowledge Dr. Dengjun Wang for his valuable suggestions.

Appendix A. Supplementary data

The supplementary information provides a brief description and discussion of: (i) determination of aggregation kinetics (S1); (ii) interaction energy calculations (S2); (iii) mathematical modeling (S3); (iv) zeta potentials of graphene oxide (GO) and quartz sand as a function of the ionic strength (Fig. S1); (v) hydrodynamic diameters of GO as a function of the IS (Fig. S2); (vi) calculated attachment efficiencies for GO aggregation as a function of the IS (Fig. S3); (vii) effect of IS (1, 50, and 100 mM NaCl) on the transport and retention of GO (Fig. S4); (viii) the retention of GO and the GO release in the background electrolyte solution after the column was turned upside down (Fig. S5); (ix) parameters for interaction energy calculations (Table S1); (x) interaction energy parameters for GO-GO and GO-sand for all solution chemistries when GO is oriented parallel to the interacting surface (Table S2); (xi) interaction energy parameters for GO-GO and GO-sand for various GO thicknesses (1 and 10 nm) and orientations (parallel and perpendicular) with the surface when the IS = 20 mM NaCl (Table S3); (xii) interaction energy parameters for GO-GO and GO-sand for all solution chemistries when GO is oriented perpendicular to the interacting surface and one of the surfaces has a roughness fraction of 0.05 and roughness of height of 30 nm (Table S4); and (xiii) interaction energy parameters for GO-GO and GO-sand for all solution chemistries when GO is oriented perpendicular to the interacting surface and both surfaces have a roughness fraction of 0.05 and roughness of height of 30 nm (Table S5). This information is available free of charge via the Internet. Supplementary data to this article can be found online at https://doi.org/10.1016/j.scitotenv.2018.11.258.

References

Baalousha, M., 2009. Aggregation and disaggregation of iron oxide nanoparticles: influence of particle concentration, pH and natural organic matter. Sci. Total Environ. 407, 2093–2101.

Bendersky, M., Davis, J.M., 2011. DLVO interaction of colloidal particles with topographically and chemically heterogeneous surfaces. J. Colloid Interface Sci. 353, 87–97.

Bhattacharjee, S., Ko, C.-H., Elimelech, M., 1998. DLVO interaction between rough surfaces. Langmuir 14, 3365–3375.

Bradford, S.A., Kim, H., 2010. Implications of cation exchange on clay release and colloid-facilitated transport in porous media. J. Environ. Qual. 39, 2040–2046.

Bradford, S.A., Leij, F.J., 2018. Modeling the transport and retention of polydispersed colloidal suspensions in porous media. Chem. Eng. Sci. 192, 972–980.

Bradford, S.A., Torkzaban, S., 2012. Colloid adhesive parameters for chemically heterogeneous porous media. Langmuir 28, 13643–13651.

Bradford, S.A., Torkzaban, S., 2013. Colloid interaction energies for physically and chemically heterogeneous porous media. Langmuir 29, 3668–3676.
Bradford, S.A., Simunek, J., Bettahar, M., van Genuchten, M.T., Yates, S.R., 2003. Modeling colloid attachment, straining, and exclusion in saturated porous media. Environ. Sci. Technol. 37, 2242–2250.
Bradford, S.A., Torkzaban, S., Leij, F., Simunek, J., 2015. Equilibrium and kinetic models for colloid release under transient solution chemistry conditions. J. Contam. Hydrol. 181, 141–152.
Bradford, S.A., Kim, H., Shen, C., Sasidharan, S., Shang, J., 2017. Contributions of nanoscale roughness to anomalous colloid retention and stability behavior. Langmuir 33, 10094–10105.
Bradford, S.A., Sasidharan, S., Kim, H., Hwang, G., 2018. Comparison of types and amounts of nanoscale heterogeneity on bacteria retention. Front. Environ. Sci. 6.
Chen, K.L., Elimelech, M., 2006. Aggregation and deposition kinetics of fullerene (C60) nanoparticles. Langmuir 22, 10994–11001.
Chowdhury, I., Duch, M.C., Mansukhani, N.D., Hersam, M.C., Bouchard, D., 2014. Deposition and release of graphene oxide nanomaterials using a quartz crystal microbalance. Environ. Sci. Technol. 48, 961–969.
Dong, S., Shi, X., Gao, B., Wu, J., Sun, Y., Guo, H., Xu, H., Wu, J., 2016. Retention and release of graphene oxide in structured heterogeneous porous media under saturated and unsaturated conditions. Environ. Sci. Technol. 50, 10397–10405.
Dong, S., Sun, Y., Gao, B., Shi, X., Xu, H., Wu, J., Wu, J., 2017. Retention and transport of graphene oxide in water-saturated limestone media. Chemosphere 180, 506–512.
Dreyer, D.R., Park, S., Bielawski, C.W., Ruoff, R.S., 2010. The chemistry of graphene oxide. Chem. Soc. Rev. 39, 228–240.
Fan, W., Jiang, X., Lu, Y., Huo, M., Lin, S., Geng, Z., 2015a. Effects of surfactants on graphene oxide nanoparticles transport in saturated porous media. J. Environ. Sci. 35, 12–19.
Fan, W., Jiang, X.H., Yang, W., Geng, Z., Huo, M.X., Liu, Z.M., Zhou, H., 2015b. Transport of graphene oxide in saturated porous media: effect of cation composition in mixed Na-Ca electrolyte systems. Sci. Total Environ. 511, 509–515.
Feriancikova, L., Xu, S., 2012. Deposition and remobilization of graphene oxide within saturated sand packs. J. Hazard. Mater. 235–236, 194–200.
Grosberg, A.Y., Nguyen, T.T., Shklovskii, B.I., 2002. Colloquium: the physics of charge inversion in chemical and biological systems. Rev. Mod. Phys. 74, 329–345.
Guo, X., Mei, N., 2014. Assessment of the toxic potential of graphene family nanomaterials. J. Food Drug Anal. 22, 105–115.
He, K., Chen, G., Zeng, G., Peng, M., Huang, Z., Shi, J., Huang, T., 2017. Stability, transport and ecosystem effects of graphene in water and soil environments. Nanoscale 9, 5370–5388.
He, K., Chen, G., Zeng, G., Chen, A., Huang, Z., Shi, J., Huang, T., Peng, M., Hu, L., 2018. Three-dimensional graphene supported catalysts for organic dyes degradation. Appl. Catal. B 228, 19–28.
Henry, C., Minier, J.-P., Lefèvre, G., Hurisse, O., 2011. Numerical study on the deposition rate of hematite particle on polypropylene walls: role of surface roughness. Langmuir 27, 4603–4612.
Hoek, E.M.V., Agarwal, G.K., 2006. Extended DLVO interactions between spherical particles and rough surfaces. J. Colloid Interface Sci. 298, 50–58.
Konopinski, D.I., Hudziak, S., Morgan, R.M., Bull, P.A., Kenyon, A.J., 2012. Investigation of quartz grain surface textures by atomic force microscopy for forensic analysis. Forensic Sci. Int. 223, 245–255.
Lanphere, J.D., Luth, C.J., Walker, S.L., 2013. Effects of solution chemistry on the transport of graphene oxide in saturated porous media. Environ. Sci. Technol. 47, 4255–4261.
Lanphere, J.D., Rogers, B., Luth, C., Bolster, C.H., Walker, S.L., 2014. Stability and transport of graphene oxide nanoparticles in groundwater and surface water. Environ. Eng. Sci. 31 (350-350).
Lee, K.W., 1983. Change of particle size distribution during Brownian coagulation. J. Colloid Interface Sci. 92, 315–325.
Leij, F.J., Bradford, S.A., Wang, Y., Sciortino, A., 2015. Langmuirian blocking of irreversible colloid retention: analytical solution, moments, and setback distance. J. Environ. Qual. 44, 1473–1482.
Liang, Y., Bradford, S.A., Simunek, J., Vereecken, H., Klumpp, E., 2013. Sensitivity of the transport and retention of stabilized silver nanoparticles to physicochemical factors. Water Res. 47, 2572–2582.
Liu, S., Zeng, T.H., Hofmann, M., Burcombe, E., Wei, J., Jiang, R., Kong, J., Chen, Y., 2011. Antibacterial activity of graphite, graphite oxide, graphene oxide, and reduced graphene oxide: membrane and oxidative stress. ACS Nano 5, 6971–6980.
Liu, L., Gao, B., Wu, L., Morales, V.L., Yang, L., Zhou, Z., Wang, H., 2013. Deposition and transport of graphene oxide in saturated and unsaturated porous media. Chem. Eng. J. 229, 444–449.
Messina, F., Marchisio, D.L., Sethi, R., 2015. An extended and total flux normalized correlation equation for predicting single-collector efficiency. J. Colloid Interface Sci. 446, 185–193.
Qi, Z., Zhang, L., Wang, F., Hou, L., Chen, W., 2014. Factors controlling transport of graphene oxide nanoparticles in saturated sand columns. Environ. Toxicol. Chem. 33, 998–1004.
Roy, S.B., Dzombak, D.A., 1996. Colloid release and transport processes in natural and model porous media. Colloids Surf. A Physicochem. Eng. Asp. 107, 245–262.
Shellenberger, K., Logan, B.E., 2002. Effect of molecular scale roughness of glass beads on colloidal and bacterial deposition. Environ. Sci. Technol. 36, 184–189.
Shen, C., Li, B., Huang, Y., Jin, Y., 2007. Kinetics of coupled primary- and secondary-minimum deposition of colloids under unfavorable chemical conditions. Environ. Sci. Technol. 41, 6976–6982.
Shen, C., Li, B., Wang, C., Huang, Y., Jin, Y., 2011. Surface roughness effect on deposition of nano- and micro-sized colloids in saturated columns at different solution ionic strengths. Vadose Zone J. 10, 1071–1081.
Shen, C., Bradford, S.A., Li, T., Li, B., Huang, Y., 2018. Can nanoscale surface charge heterogeneity really explain colloid detachment from primary minima upon reduction of solution ionic strength? J. Nanopart. Res. 20, 165.
Šimůnek, J., van Genuchten, M.T., Šejna, M., 2016. Recent developments and applications of the HYDRUS computer software packages. Vadose Zone J. 15, 1539–1663.
Sun, Y., Gao, B., Bradford, S.A., Wu, L., Chen, H., Shi, X., Wu, J., 2015. Transport, retention, and size perturbation of graphene oxide in saturated porous media: effects of input concentration and grain size. Water Res. 68, 24–33.
Suresh, L., Walz, J.Y., 1996. Effect of surface roughness on the interaction energy between a colloidal sphere and a flat plate. J. Colloid Interface Sci. 183, 199–213.
Torkzaban, S., Bradford, S.A., 2016. Critical role of surface roughness on colloid retention and release in porous media. Water Res. 88, 274–284.
Torkzaban, S., Kim, Y., Mulvihill, M., Wan, J., Tokunaga, T.K., 2010. Transport and deposition of functionalized CdTe nanoparticles in saturated porous media. J. Contam. Hydrol. 118, 208–217.
Torkzaban, S., Wan, J., Tokunaga, T.K., Bradford, S.A., 2012. Impacts of bridging complexation on the transport of surface-modified nanoparticles in saturated sand. J. Contam. Hydrol. 136–137, 86–95.
Wang, S., Sun, H., Ang, H.M., Tadé, M.O., 2013. Adsorptive remediation of environmental pollutants using novel graphene-based nanomaterials. Chem. Eng. J. 226, 336–347.
Wang, D., Shen, C., Jin, Y., Su, C., Chu, L., Zhou, D., 2017a. Role of solution chemistry in the retention and release of graphene oxide nanomaterials in uncoated and iron oxide-coated sand. Sci. Total Environ. 579, 776–785.
Wang, M., Gao, B., Tang, D., Sun, H., Yin, X., Yu, C., 2017b. Effects of temperature on graphene oxide deposition and transport in saturated porous media. J. Hazard. Mater. 331, 28–35.
Wang, M., Gao, B., Tang, D., Yu, C., 2018. Concurrent aggregation and transport of graphene oxide in saturated porous media: roles of temperature, cation type, and electrolyte concentration. Environ. Pollut. 235, 350–357.
Wu, L., Gao, B., Tian, Y., Muñoz-Carpena, R., Zigler, K.J., 2013a. DLVO interactions of carbon nanotubes with isotropic planar surfaces. Langmuir 29, 3976–3988.
Wu, L., Liu, L., Gao, B., Muñoz-Carpena, R., Zhang, M., Chen, H., Zhou, Z., Wang, H., 2013b. Aggregation kinetics of graphene oxides in aqueous solutions: experiments, mechanisms, and modelling. Langmuir 29, 15174–15181.
Xia, T., Fortner, J.D., Zhu, D., Qi, Z., Chen, W., 2015. Transport of sulfide-reduced graphene oxide in saturated quartz sand: cation-dependent retention mechanisms. Environ. Sci. Technol. 49, 11468–11475.
Xia, J., Li, F., Ji, S., Xu, H., 2017. Selenium-functionalized graphene oxide that can modulate the balance of reactive oxygen species. ACS Appl. Mater. Interfaces 9, 21413–21421.
Zhang, M., Bradford, S.A., Šimůnek, J., Vereecken, H., Klumpp, E., 2016. Do goethite surfaces really control the transport and retention of multi-walled carbon nanotubes in chemically heterogeneous porous media? Environ. Sci. Technol. 50, 12713–12721.
Zhu, Y., Murali, S., Cai, W., Li, X., Ji, W.S., Potts, J.R., Ruoff, R.S., 2010. Graphene-based materials: graphene and graphene oxide: synthesis, properties and applications. Adv. Mater. 22, 3906–3924.